Geomechanics and Engineering, *Vol. 42, No. 3 (2025) 191-206*
https://doi.org/10.12989/gae.2025.42.3.191

On the bending behavior of porous functionally graded plates under hygro-thermo-mechanical loads

Baghdad Hassaine Daouadji[1], Amina Attia[2], Abdelmoumen Anis Bousahla[3], Abdelouahed Tounsi*[1,4], Abdeldjebbar Tounsi[1,5], Sherain M.Y. Mohamed[6], Saad Althobaiti[7], Mahmoud M. Selim[6], Murat Yaylacı[8,9] and Salem Mohammed Aldosari[10,11]

[1]*Material and Hydrology Laboratory, Faculty of Technology, Civil Engineering Department, University of Sidi Bel Abbes, Algeria*
[2]*Department of Civil Engineering and Public Works, Engineering and Sustainable Development Laboratory, Faculty of Science and Technology, University of Ain Temouchent, Algeria*
[3]*Laboratoire de Modélisation et Simulation Multi-échelle, Université de Sidi Bel Abbés, Algeria*
[4]*Department of Civil and Environmental Engineering, King Fahd University of Petroleum & Minerals, 31261 Dhahran, Eastern Province, Saudi Arabia*
[5]*Mechanical Engineering Department, Faculty of Science and Technology, University of Rélizane, Relizane, Algeria*
[6]*Department of Mathematics, College of Science and Humanities, Prince Sattam bin Abdulaziz University, Al-Kharj 11942, Saudi Arabia*
[7]*Department of Sciences and Technology, Ranyah University Collage, Taif University, P.O. Box 11099, Taif 21944, Saudi Arabia*
[8]*Department of Civil Engineering, Recep Tayyip Erdogan University, 53100, Rize, Turkey*
[9]*Faculty of Turgut Kıran Maritime, Recep Tayyip Erdogan University, 53900, Rize, Turkey*
[10]*Material Science Research Institute, King Abdulaziz City for Science and Technology (KACST), Riyadh 11442, Saudi Arabia*
[11]*Composites and Advanced Materials Centre, School of Aerospace, Transport and Manufacturing, Cranfield University, Cranfield MK43 0AL, UK*

(*Received February 4, 2025, Revised July 10, 2025, Accepted July 11, 2025*)

Abstract. This investigation focuses on the static behavior of an advanced porous functionally graded (FG) plate with varying material composition, subjected to combined mechanical, thermal, and moisture loads while resting on a viscoelastic foundation. A modified first-order shear deformation theory (FSDT), enhanced by a shear distribution function, is employed to more accurately capture out-of-plane shear deformation. The variation of elastic properties through the plate's thickness is described using a power-law distribution. The effects of temperature and moisture on the material properties are assumed to be linear and are incorporated into the analysis to evaluate their influence on the plate's bending behavior. The viscoelastic foundation is modeled using three parameters: Winkler's modulus, Pasternak's shear coefficient, and a damping coefficient. The governing equations are derived using the principle of virtual displacement and solved analytically using the Navier method under simply supported boundary conditions. The nondimensional numerical results are validated through comparison with existing literature. A detailed parametric study is conducted to examine the effects of the gradient index, porosity index, temperature variation, moisture concentration, and damping coefficient on the bending response of the FG plate. The results demonstrate the complex interactions between these parameters and confirm the robustness and effectiveness of the proposed model in evaluating the mechanical performance of FG structures under realistic environmental and mechanical loading conditions.

Keywords: bending; modified first shear deformation theory; porous ceramic-metal plate; viscoelastic base

1. Introduction

Functionally graded material (FGM) is a composite material comprising a blend of metal and ceramic, intentionally designed with varying volume fractions of the two materials across a structure's surfaces. The mechanical characteristics, which include Young's modulus, Poisson's ratio, shear modulus of elasticity, material density, and both thermal and moisture expansion, exhibit a gradual and uninterrupted variation across functionally graded (FG) plates. These attributes commonly involve engineering alloys such as aluminum, magnesium, titanium, copper, steel, and tungsten, alongside advanced structural ceramics like alumina, zirconia, tungsten carbide, and silicon carbide (Birman and Byrd 2007, Mantari and Soares 2013, Carrera *et al.* 2008). Investigating the effects of moisture and temperature on the deformation and stress within various plate structures has garnered considerable scholarly attention, as demonstrated by the contributions of researchers including Ram and Sinha 1991, Patel *et al.* 2002, Shen 2001, Rao and Sinha 2004, Benkhedda *et al.* 2008, Lo *et al.* 2010, Wang *et al.* 2005, Cinefra *et al.* 2017, Pham *et al.* 2024, Shankar *et al.* 2017, Bot *et al.* 2022, Tounsi *et al.* 2023, Yuksel and Akbas 2021, Ebrahimi *et al.* 2019, Zhang *et al.* 2023. This context underscores the importance of ongoing research in this field. Elastic foundation structures are widely used in modern engineering and present significant technical challenges in structural design. The interaction between the FG plate and the foundation is commonly represented by the Winkler

*Corresponding author, Professor
E-mail: tou_abdel@yahoo.com

ISSN: 2005-307X (Print), 2092-6219 (Online)

model, also known as the one-parameter model, first introduced by Winkler in 1867. The Winkler model was further improved with the addition of a "shear spring" to create the "Pasternak model". The formula for the Pasternak (1954) elastic model has been adjusted to take into account the deflection caused by creep by incorporating a damping parameter (Kerr 1964).

A multitude of theories have been employed to scrutinize plate behavior (Gupta and Talha 2015). The classical plate theory (Leissa 1973) stands out as an effective approach for thin plates. In the analysis of plate mechanics, it is observed that thicker plates necessitate the application of higher-order shear deformation theories. Specifically, Mindlin's (Mindlin 1951) first-order shear deformation theory, proposed in 1951, and Reddy's third-order shear deformation theory are pertinent in this context. A significant amount of scholarly work has been dedicated to the examination of plates, particularly those made from functionally graded materials. Key contributions to this field include studies by Zghal *et al*. (2017), Tu *et al.* (2017), Li *et al.* (2020), Nguyen *et al.* (2015), Baseri *et al*. (2016), Arefi and Meskini (2019), Adim and Daouadji (2016), Ebrahimi and Habibi (2016), Rabhi *et al*. (2020), and Turan (2024).

Numerous researchers have extensively examined and studied the behavior of imperfect functionally graded plates, especially those with inherent porosity, as a captivating topic in the literature (Arshid and Khorshidvand 2018, Barati 2018, Avcar 2019, Akbaş 2021, Rostami *et al*. 2020, Mohammadimehr *et al*. 2020, Ahmed *et al*. 2020, Rahimi *et al*. 2020, Beg *et al*. 2021, Huang and Tahouneh 2021, Madenci and Özkılıç 2021, Tlidji *et al*. 2021, Keleshteri and Jelovica 2021, Khorshidvand *et al*. 2014, Feyzi and Khorshidvand 2017, Cong *et al*. 2018, Ahmed *et al*. 2019, Hamed *et al*. 2020, Ebrahimi *et al*. 2020, Priyanka *et al.* 2021, Cho 2023, Jain and Azam 2024, Çapar *et al.* 2024).

The recent literature presents extensive research on the behavior of porous functionally graded material (FGM) plates using advanced shear deformation theories and meshfree methods. Sharma *et al.* (2024) investigated the impact of porosity on the stability of bidirectional FGM skew plates using a higher-order shear deformation theory (HSDT) combined with the radial basis function (RBF) approach, emphasizing the role of porosity in structural stability. Kumar *et al.* (2023a) conducted a geometrically nonlinear analysis of FG plates under patch loading, revealing the influence of gradient properties on flexural response. In another study, Kumar *et al.* (2023b) used the RBF collocation method to analyze the free vibration of elastically supported porous bidirectional FGM plates with different porosity distributions. Kumar *et al.* (2023c) proposed a new tangent HSDT for porosity-dependent buckling analysis of FGM sandwich plates on elastic foundations using a meshfree technique. Additionally, Kumar *et al.* (2022a) presented a meshfree bending analysis of porous rectangular FG plates resting on elastic foundations, while Kumar *et al*. (2022b) addressed flexure behavior under various transverse loads. Other notable works include vibration analysis of porous FGM sandwich plates using collocation methods (Kumar *et al.* 2022c), thermomechanical buckling simulations (Kumar *et al.* 2022d, e), and buckling/free vibration studies incorporating new shear theories (Kumar *et al*. 2019a, b). Collectively, these contributions highlight the importance of advanced modeling approaches such as HSDTs, porosity modeling, and meshfree numerical methods in capturing the complex mechanical behavior of porous FG plates, offering valuable insights for the design of next-generation engineering structures. Khider *et al.* (2024) provide a comprehensive review on nonlocal porous FG nanobeams subjected to moving loads, highlighting recent advancements in dynamic analysis. Ahmed *et al.* (2021) examine the thermal and dynamic responses of FG porous piezoelectric plates using nonlocal theories. Al-Toki *et al*. (2021) investigate the effects of impulse and thermal loads on nonlocal porous graded beams, offering insights into their vibration characteristics. Hamad *et al.* (2019) focus on both static and dynamic analyses of strain gradient porous nano-crystalline shell structures. These studies underscore the importance of advanced modeling techniques such as nonlocal elasticity and strain gradient theories in accurately predicting the complex behavior of nanostructures exposed to dynamic and thermal environments. Hamed *et al*. (2019) conducted an analysis on the mechanical bending behavior of a flawed FG nanobeam with four different porosity distributions using nonlocal elasticity and Euler-Bernoulli beam theory. In a similar vein, Hadji *et al.* (2020) investigated how the porosity distribution model impacts the static response of a functionally graded beam, employing a novel HSDT formulation as the basis for their study. The topic of porosity distribution in these studies is of particular interest in understanding the structural behavior of these materials. The investigation conducted by Adim and Daouadji (2024) focuses on the effects of hygro-thermo-mechanical loading and the micromechanical model on the bending characteristics of functionally graded material (FGM) plates supported by Winkler and Pasternak elastic foundations.

This research employs higher-order shear deformation theory to analyze the subject matter. Additionally, Daouadji and Benferhat (2016) previously conducted an analysis on the flexural bending of FGM plates, taking into account both ideal and flawed conditions under hygro-thermo-mechanical stresses. Although there is a comprehensive body of literature regarding the bending behavior of FGM plates utilizing various theoretical frameworks and loading scenarios, the response characteristics of these plates situated on a viscoelastic foundation under nonlinear hygro-thermo-mechanical influences remain largely underexplored. Therefore, the current study seeks to fill this gap by systematically examining the bending response of FGM plates resting on viscoelastic foundations subjected to hygro-thermo-mechanical loads, utilizing a higher-order integral shear deformation theory that incorporates only four variables.

The objectives of this research are to analyze the bending behavior of functionally graded (FG) ceramic-metal porous plates subjected to combined humidity and temperature variations while resting on a three-parameter elastic foundation; to develop and implement a simplified first- order shear deformation theory (FSDT) involving only

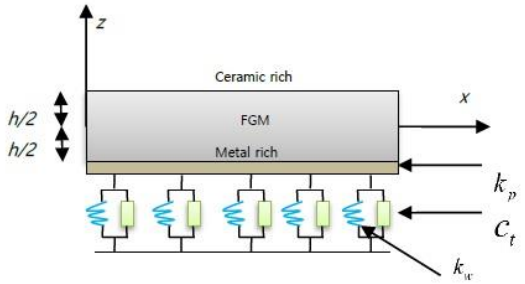

Fig. 1 A typical ceramic-metal plate specifically created for FGM, positioned over a viscoelastic foundation.

four unknown displacement functions, thereby reducing computational effort compared to more complex models; to account for temperature- and moisture-dependent material properties in modeling imperfect FG plates; to derive the governing equilibrium equations using the principle of virtual work within the proposed theoretical framework; and to perform a comprehensive parametric study evaluating the influence of porosity, gradient index, and foundation parameters. The outcomes are compared with existing results for both perfect and imperfect FG plates to validate the model and demonstrate its effectiveness. The incorporation of a viscoelastic foundation makes the model relevant for applications involving layered systems, such as pavement structures, sandwich panels, and bio-inspired composite materials, where damping and foundation interactions play a critical role in structural stability and service life.

2. Theoretical formulations

The theoretical formulation considers a rectangular functionally graded porous (FGP) plate with precisely defined dimensions: length, width, and thickness. The plate is simply supported along its edges, and a Cartesian coordinate system (x, y, z) is used, where the x and y axes correspond to the in-plane dimensions (length and width), and the z axis represents the thickness direction, as shown in Fig. 1. The positions of the top and bottom surfaces of the plate are clearly defined, providing a consistent reference for the application of boundary conditions and the variation of material properties through the thickness.

In this work, the power law distribution of the volume fraction is used to represent the change of material properties in FGMs. The porosity phases distribute uniformly over the entire cross section. This model was developed by Wattanasakulpong and Ungbhakorn (2014) where the porosity is constant across the thicknesses of the FG-plate. The Young's modulus is represented as follows

$$E(z) = (E_c - E_m)V_c + E_m - \frac{xi}{2}(E_c + E_m) \qquad (1)$$

$$\text{and } V_c(z) = \left(\frac{z}{h} + \frac{1}{2}\right)^p$$

xi denotes the porosity fraction index, distributed equally in the metal and ceramic phases. c and m are related to the pure ceramic and metal plates, respectively.

2.1 Field of displacement and deformations

The displacement field and strains formulated in the present First-Order Shear Deformation Theory (FSDT) rely on particular foundational assumptions. These assumptions entail the separation of transverse displacement into components corresponding to bending and shear, alongside the division of in-plane displacements into their extension and bending constituents. Furthermore, it is noteworthy that the bending components of the in-plane displacements exhibit similarities to those delineated in Classical Plate Theory (CPT). Overall, the displacement field articulated within this theoretical framework is characterized by a thorough and generalized representation.

$$\begin{aligned} u(x,y,z) &= u_0(x,y) - z\frac{\partial w_b}{\partial x} \\ v(x,y,z) &= v_0(x,y) - z\frac{\partial w_b}{\partial y} \\ w(x,y,z) &= w_b(x,y) + w_s(x,y) \end{aligned} \qquad (2a)$$

The displacements along the x and y coordinate directions of a point on the mid-plane of the plate are indicated by u_0 and v_0 ; while the bending and shear components of the transverse displacement are denoted by w_b and w_s . The strains associated with the displacement field in Eq. (2(a)) are

$$\begin{Bmatrix} \varepsilon_x \\ \varepsilon_y \\ \gamma_{xy} \\ \gamma_{yz} \\ \gamma_{xz} \end{Bmatrix} = \begin{Bmatrix} \dfrac{\partial u_0}{\partial x} + z\left(-\dfrac{\partial^2 w_b}{\partial x^2}\right) \\ \dfrac{\partial v_0}{\partial x} + z\left(-\dfrac{\partial^2 w_b}{\partial y^2}\right) \\ \dfrac{\partial u_0}{\partial y} + \dfrac{\partial v_0}{\partial x} + \left(-2z\dfrac{\partial^2 w_b}{\partial x \partial y}\right) \\ \gamma_{yz}^s \\ \gamma_{xz}^s \end{Bmatrix} \qquad (2b)$$

In the traditional formulation of the First-order Shear Deformation Theory (FSDT), the shear strain is assumed to vary linearly throughout the material's thickness, necessitating the introduction of a shear correction factor. In contrast, the actual distribution of shear stress exhibits a parabolic profile across the thickness, diminishing to zero at both the upper and lower surfaces. This study proposes a new function for the distribution of shear to enhance the simplified FSDT. Consequently, this leads to the derivation of the shear strain vector as follows

$$\begin{Bmatrix} \gamma^c{}_{yz} \\ \gamma^c{}_{xz} \end{Bmatrix} = g(z)\begin{Bmatrix} \gamma_{yz} \\ \gamma_{xz} \end{Bmatrix} \qquad (3)$$

The function required $g(z)$ describes how the transverse shear strains are distributed throughout the thickness of the plate. This shear distribution function is specifically selected to comply with the stress-free boundary conditions at both the upper and lower surfaces of the plate. Furthermore, the integration across the thickness parallels

the approach taken with the constant shear correction factor utilized in the First-Order Shear Deformation Theory (FSDT), which is represented by a value of 5/6. The shear distribution function used in this study differs from that of Zenkour (2006) by offering a simplified form within a modified first-order shear deformation theory (FSDT), involving only four displacement variables. While Zenkour's model employs a higher-order hyperbolic function to avoid shear correction factors, our approach introduces a tailored shear function that enhances accuracy while preserving computational efficiency. Consequently, the shear distribution function may be defined as (Zenkour 2006, Nguyen *et al.* 2019)

$$g(z)=\frac{5}{4}cos\left(\frac{\pi z}{h}\right) \tag{4}$$

2.2 stress-strain relationships

The material is isotropic at each point, The stress-strain relationships associated with the FG plates, specifically in a plane-stress condition, can be expressed as follows

$$\begin{Bmatrix}\sigma_x\\ \sigma_y\\ \tau_{yz}\\ \tau_{xz}\\ \tau_{xy}\end{Bmatrix}=\begin{bmatrix}C_{11} & C_{12} & 0 & 0 & 0\\ C_{12} & C_{22} & 0 & 0 & 0\\ 0 & 0 & C_{44} & 0 & 0\\ 0 & 0 & 0 & C_{55} & 0\\ 0 & 0 & 0 & 0 & C_{66}\end{bmatrix} \times \begin{Bmatrix}\varepsilon_x-\alpha(z)\,\Delta T-\beta(z)\,\Delta C\\ \varepsilon_y-\alpha(z)\,\Delta T-\beta(z)\,\Delta C\\ \gamma_{yz}\\ \gamma_{xz}\\ \gamma_{xy}\end{Bmatrix} \tag{5}$$

where

$$C_{11}=C_{22}=\frac{E(z)}{1-\nu(z)^2}$$

$$C_{12}=\nu(z)\,C_{11} \tag{6}$$

$$C_{44}=C_{55}=C_{66}=\frac{E(z)}{2(1+\nu(z))}$$

We consider the plate under a thermal field and moisture concentration varying linearly within the thickness, i.e., $T(x,y,z)=T_1(x,y)+\frac{z}{h}T_2(x,y)$ and $C(x,y,z)=C_1(x,y)+\frac{z}{h}C_2(x,y)$.

3. Governing equations

After the formulation of the strain and stress tensors, the principle of virtual work is utilized to formulate the governing differential equations. Initially, this principle involves calculating the integral of the product of the stress and the variation of strain within the xy domain. This is then followed by integration through the thickness of the plate, as illustrated in Eq. (7).

$$\int_{-h/2}^{h/2}\int_{\Omega}\left[\sigma_x\delta\,\varepsilon_x+\sigma_y\delta\,\varepsilon_y+\tau_{xy}\delta\,\gamma_{xy}+\tau_{xz}\delta\,\gamma_{xz}+\tau_{yz}\delta\,\gamma_{yz}\right]d\,\Omega\,d\,z-\int_{\Omega}(q-f_e)\,\delta\,w\,d\,\Omega=0 \tag{7}$$

In the Eq. (7), q represents the mechanical load applied in the transverse direction (z) of the plate, while *f*e denotes the force exerted by the foundation. The characterization of the force follows the viscoelastic Winkler-Pasternack model, as presented in Eq. (8).

$$f_e=\left(k_w-k_p\nabla^2+c_t\frac{\partial}{\partial t}\right)w(x,y) \tag{8}$$

k_w, k_p and c_t represents Winkler parameter, the shear layer foundation stiffness and viscosity parameter, respectively.

Substituting Eqs. (2) and (5) into Eq. (7) and integrating across the thickness of the plate, Eq. (7) can be expressed as

$$\int_{\Omega}\left[N_x\delta\,\varepsilon_x^0+N_y\delta\,\varepsilon_y^0+N_{xy}\delta\,\varepsilon_{xy}^0+M_x^b\delta\,k_x^b+M_y^b\delta\,k_y^b+M_{xy}^b\delta\,k_{xy}^b+S_{yz}^s\gamma_{yz}^s+S_{xz}^s\gamma_{xz}^s\right]d\,\Omega-\int_{\Omega}(q-f_e)\,\delta\,w\,d\,\Omega=0 \tag{9}$$

N, M and S are stress resultants and can be expressed as follows

$$\begin{Bmatrix}N_x & N_y & N_{xy}\\ M_x^b & M_y^b & M_{xy}^b\end{Bmatrix}=\int_{-h/2}^{h/2}\left(\sigma_x,\sigma_y,\tau_{xy}\right)\begin{Bmatrix}1\\ z\end{Bmatrix}dz \tag{10a}$$

$$\left(S_{xz}^s,S_{yz}^s\right)=\int_{-h/2}^{h/2}\left(\tau_{xz},\tau_{yz}\right)g(z)dz \tag{10b}$$

Substituting Eq. (5) into Eq. (10) and integrating across the thickness of the plate, the stress resultants are written as

$$\begin{Bmatrix}\begin{Bmatrix}N_x\\ N_y\\ N_{xy}\end{Bmatrix}\\ \begin{Bmatrix}M_x^b\\ M_y^b\\ M_{xy}^b\end{Bmatrix}\end{Bmatrix}=\begin{bmatrix}\begin{bmatrix}A_{11} & A_{12} & 0\\ A_{12} & A_{22} & 0\\ 0 & 0 & A_{66}\end{bmatrix} & \begin{bmatrix}B_{11} & B_{12} & 0\\ B_{12} & B_{22} & 0\\ 0 & 0 & B_{66}\end{bmatrix}\\ \begin{bmatrix}B_{11} & B_{12} & 0\\ B_{12} & B_{22} & 0\\ 0 & 0 & B_{66}\end{bmatrix} & \begin{bmatrix}D_{11} & D_{12} & 0\\ D_{12} & D_{22} & 0\\ 0 & 0 & D_{66}\end{bmatrix}\end{bmatrix}\begin{Bmatrix}\begin{Bmatrix}\varepsilon_x^0\\ \varepsilon_y^0\\ \gamma_{xy}^0\end{Bmatrix}\\ \begin{Bmatrix}k_x^b\\ k_y^b\\ k_{xy}^b\end{Bmatrix}\end{Bmatrix}-\begin{Bmatrix}\begin{Bmatrix}N_x^T\\ N_y^T\\ 0\end{Bmatrix}\\ \begin{Bmatrix}M_x^{bT}\\ M_y^{bT}\\ 0\end{Bmatrix}\end{Bmatrix}-\begin{Bmatrix}\begin{Bmatrix}N_x^C\\ N_y^C\\ 0\end{Bmatrix}\\ \begin{Bmatrix}M_x^{bC}\\ M_y^{bC}\\ 0\end{Bmatrix}\end{Bmatrix} \tag{11a}$$

$$\begin{Bmatrix}S_{yz}^s\\ S_{xz}^s\end{Bmatrix}=\begin{bmatrix}A_{44}^s & 0\\ 0 & A_{55}^s\end{bmatrix}\begin{Bmatrix}\gamma_{yz}^0\\ \gamma_{xz}^0\end{Bmatrix} \tag{11b}$$

and stiffness components are given as

$$(A_{ij}, B_{ij}, D_{ij}) = \int_{-h/2}^{h/2} C_{ij}(1, z, z^2)dz, \ (i, j = 1,2,6), \quad (12a)$$

$$A_{ij}^s = \int_{-h/2}^{h/2} C_{ij}\left[g(z)\right]^2 dz, \ \ (i, j = 4,5) \quad (12b)$$

The hygrothermal stress and moment resultants $N_x^\theta = N_y^\theta$, $M_x^{b\theta} = M_y^{b\theta}$ and $M_x^{s\theta} = M_y^{s\theta}$ are defined by

$$\left[N_x^\theta, M_x^{b\theta}\right] = \int_{-h/2}^{h/2} \frac{E(z)}{1-\nu} \left[1, z,\right] \eta \ \theta \ dz \quad (13)$$

where

$$\theta = \begin{cases} T \ \text{ if } \ \eta = \alpha, \\ C \ \text{ if } \ \eta = \beta, \end{cases} \quad (14)$$

The governing equations of equilibrium can be obtained from Eq. (9) by integrating the displacement gradients by parts and setting the coefficients δu_0, δv_0, δw_b and δw_s zero separately. Thus one can obtain the equilibrium equations associated with the present theory

$$\begin{aligned} &\delta u_0: \ \frac{\partial N_x}{\partial x} + \frac{\partial N_{xy}}{\partial y} = 0 \\ &\delta v_0: \ \frac{\partial N_{xy}}{\partial x} + \frac{\partial N_y}{\partial y} = 0 \\ &\delta w_b: \ \frac{\partial^2 M_x^b}{\partial x^2} + 2\frac{\partial^2 M_{xy}^b}{\partial x \partial y} + \frac{\partial^2 M_y^b}{\partial y^2} - f_e + q = 0 \\ &\delta w_s: \ \frac{\partial^2 M_x^s}{\partial x^2} + 2\frac{\partial^2 M_{xy}^s}{\partial x \partial y} + \frac{\partial^2 M_y^s}{\partial y^2} + \frac{\partial S_{xz}^s}{\partial x} + \frac{\partial S_{yz}^s}{\partial y} - f_e \\ &\qquad + q = 0 \end{aligned} \quad (15)$$

Substituting Eq. (15) into Eq. (9), the governing equations can be expressed in terms of displacements (u_0, v_0, w_b, w_s) as follows

$$\begin{aligned} &A_{11}d_{11}u_0 + A_{66}d_{22}u_0 + (A_{12} + A_{66})d_{12}v_0 \\ &\qquad - B_{11}d_{111}w_b \\ &\qquad - (B_{12} + 2B_{66})d_{122}w_b = p_1 \end{aligned} \quad (16a)$$

$$\begin{aligned} &A_{22}d_{22}v_0 + A_{66}d_{11}v_0 + (A_{12} + A_{66})d_{12}u_0 \\ &\qquad - B_{22}d_{222}w_b \\ &\qquad - (B_{12} + 2B_{66})d_{112}w_b = p_2 \end{aligned} \quad (16b)$$

$$\begin{aligned} &B_{11}d_{111}u_0 + (B_{12} + 2B_{66})d_{122}u_0 \\ &\qquad + (B_{12} + 2B_{66})d_{112}v_0 + B_{22}d_{222}v_0 \\ &\qquad - D_{11}d_{1111}w_b \\ &\qquad - 2(D_{12} + 2D_{66})d_{1122}w_b \\ &\quad - D_{22}d_{2222}w_b = p_3 \end{aligned} \quad (16c)$$

$$A_{55}^s d_{11}w_s + A_{44}^s d_{22}w_s = p_4 \quad (16d)$$

Where

$$\begin{aligned} &d_{ij} = \frac{\partial^2}{\partial x_i \partial x_j}, \ d_{ijl} = \frac{\partial^3}{\partial x_i \partial x_j \partial x_l}, \\ &d_{ijlm} = \frac{\partial^4}{\partial x_i \partial x_j \partial x_l \partial x_m}, \ d_i = \frac{\partial}{\partial x_i}, \ (i, j, l, m = 1,2). \end{aligned} \quad (17a)$$

and

$$p_1 = \frac{\partial N_x^T}{\partial x} + \frac{\partial N_x^C}{\partial x}, \ p_2 = \frac{\partial N_y^T}{\partial y} + \frac{\partial N_y^C}{\partial y}, \quad (17b)$$

$$p_3 = f_e - q + \frac{\partial^2 (M_x^{bT} + M_x^{bC})}{\partial x^2} + \frac{\partial^2 (M_y^{bT} + M_y^{bC})}{\partial y^2}$$

$$p_4 = f_e - q \quad (17c)$$

4. Analytical solution

This study aims to obtain the exact solution of Eqs. (16) for a simply supported plate. The boundary conditions relevant to this type of plate can be referenced in the works of Thai and Vo (2013). The Navier solution is applied to account for mechanical, thermal, and moisture loads (q, T_i and C_i), and it is expressed as a double Fourier series.

$$\begin{Bmatrix} q \\ T_i \\ C_i \end{Bmatrix} = \begin{Bmatrix} q_0 \\ t_i \\ c_i \end{Bmatrix} \sin(\lambda x)\sin(\mu y) \quad (i = 1, 2, 3) \quad (18)$$

where $\lambda = \pi / a$, $\mu = \pi / b$,

Following the Navier method, we suppose the following solution form for u_0, v_0, w_b and w_s that respects the boundary conditions,

$$\begin{Bmatrix} u_0 \\ v_0 \\ w_b \\ w_s \end{Bmatrix} = \begin{Bmatrix} U\cos(\lambda x)\sin(\mu y) \\ V\sin(\lambda x)\cos(\mu y) \\ W_b \sin(\lambda x)\sin(\mu y) \\ W_s \sin(\lambda x)\sin(\mu y) \end{Bmatrix}, \quad (19)$$

where U, V, W_b, and W_s are arbitrary coefficients to be determined. One obtains the following equation

$$\left[K\right]\{\Delta\} = \{P\}, \quad (20)$$

where $\{\Delta\} = \{U, V, W_b, W_s\}^t$ and $\left[K\right]$ is the symmetric matrix defined by

$$\left[K\right] = \begin{bmatrix} k_{11} & k_{12} & k_{13} & k_{14} \\ k_{12} & k_{22} & k_{23} & k_{24} \\ k_{13} & k_{23} & k_{33} & k_{34} \\ k_{14} & k_{24} & k_{34} & k_{44} \end{bmatrix} \quad (21)$$

in which

$$\begin{aligned} k_{11} &= -(A_{11}\lambda^2 + A_{66}\mu^2) \\ k_{12} &= -\lambda\mu\,(A_{12} + A_{66}) \end{aligned} \quad (22)$$

Table 1 non-dimensional deflections of FGM square ($b = a$) plates under hygro-thermo-mechanical loading. ($q0 = 100$, $t_1=c_1=0$)

p	k_w	k_p	t_2	c_2	$a/h = 5$		$a/h = 10$		$a/h = 20$	
					Sayyad and Ghugal (2019)	Present	Sayyad and Ghugal (2019)	Present	Sayyad and Ghugal (2019)	Present
0	100	0	0	0	0.2350	0.2426	0.2122	0.2142	0.2062	0.2068
			10	100	1.8390	1.8386	0.6251	0.6281	0.3107	0.3112
	0	100	0	0	0.0434	0.0437	0.0426	0.0427	0.0424	0.0424
			10	100	0.3404	0.3315	0.1256	0.1253	0.0638	0.0639
	100	100	0	0	0.0416	0.0419	0.0409	0 .0410	0.0407	0.0407
			10	100	0.3262	0.3176	0.1208	0.1202	0.0612	0.0613
1	100	0	0	0	0.2862	0.2947	0.2607	0.2630	0.2540	0.2546
			10	100	2.4129	2.4078	0.8115	0.8150	0.3936	0.3942
	0	100	0	0	0.0450	0.0452	0.0443	0.0444	0.0441	0.0441
			10	100	0.3806	0.3692	0.1383	0.1375	0.0683	0.0683
	100	100	0	0	0.0430	0.0432	0.0424	0.0425	0.0422	0.0423
			10	100	0.3630	0.3532	0.1320	0.1317	0.0654	0.0654
2	100	0	0	0	0.3007	0.3101	0.2732	0.2757	0.2659	0.2666
			10	100	2.5118	2.5058	0.8483	0.8520	0.4118	0.4125
	0	100	0	0	0.0453	0.0455	0.0446	0.0447	0.0444	0.0445
			10	100	0.3786	0.3680	0.1386	0.1382	0.0688	0.0688
	100	100	0	0	0.0434	0.0436	0.0427	0.0428	0.0425	0.0426
			10	100	0.3623	0.3520	0.1327	0.1323	0.0659	0.0659
5	100	0	0	0	0.3154	0.3258	0.2854	0.2883	0.2774	0.2782
			10	100	2.6252	2.6176	0.8892	0.8931	0.4308	0.4316
	0	100	0	0	0.0456	0.0459	0.0449	0.0450	0.0447	0.0448
			10	100	0.3800	0.3684	0.1400	0.1395	0.0695	0.0695
	100	100	0	0	0.0436	0.0438	0.0430	0.0431	0.0428	0.0429
			10	100	0.3634	0.3523	0.1340	0.1335	0.0665	0.0665
∞	100	0	0	0	0.3519	0.3614	0.3224	0.3251	0.3146	0.3154
			10	100	2.9516	2.9351	1.0017	1.0052	0.4872	0.4878
	0	100	0	0	0.0463	0.0465	0.0458	0.0458	0.0456	0.0456
			10	100	0.3888	0.3892	0.1422	0.1466	0.0706	0.0706
	100	100	0	0	0.0443	0.0449	0.0437	0.0437	0.0436	0.0435
			10	100	0.3716	0.3730	0.1360	0.1380	0.0675	0.1381

$$
\begin{aligned}
k_{13} &= \lambda\left[B_{11}\lambda^2 + (B_{12} + 2B_{66})\,\mu^2\right] \\
k_{14} &= 0 \\
k_{22} &= -(A_{66}\lambda^2 + A_{22}\mu^2) \\
k_{23} &= \mu\left[(B_{12} + 2B_{66})\,\lambda^2 + B_{22}\mu^2\right] \\
k_{24} &= 0 \\
k_{33} &= -\big(D_{11}\lambda^4 + 2(D_{12} + 2D_{66})\lambda^2\mu^2 + D_{22}\mu^4 + k_w \\
&\quad + k_p(\lambda^2 + \mu^2) + c_t\omega_f\big) \\
k_{34} &= -\big(+k_w + k_p(\lambda^2 + \mu^2) + c_t\omega_f\big) \\
k_{44} &= -\big(A_{55}^s\lambda^2 + A_{44}^s\mu^2 + k_w + k_p(\lambda^2 + \mu^2) \\
&\quad + c_t\omega_f\big)
\end{aligned}
\tag{22}
$$

The components of the generalized force vector $\{P\} = \{P_1, P_2, P_3, P_4\}^t$ are given by

$$
\begin{aligned}
P_1 &= \lambda\left[(A^T t_1 + B^T t_2) + (A^C c_1 + B^C c_2)\right], \\
P_2 &= \mu\left[(A^T t_1 + B^T t_2) + (A^C c_1 + B^C c_2)\right], \\
P_3 &= -q_0 - h(\lambda^2 + \mu^2)\left[(B^T t_1 + D^T t_2)\right. \\
&\quad \left. + (B^C c_1 + D^C c_2)\right], \\
P_4 &= -q_0
\end{aligned}
\tag{23}
$$

where

$$
\begin{aligned}
\left\{A^T, B^T, D^T\right\} &= \int_{-h/2}^{h/2} \frac{E(z)}{1-\nu}\alpha(z)\left\{1, z, z^2\right\}dz \\
\left\{A^C, B^C, D^C\right\} &= \int_{-h/2}^{h/2} \frac{E(z)}{1-\nu}\beta(z)\left\{1, z, z^2\right\}dz,
\end{aligned}
\tag{24}
$$

in which

Table 2 non-dimensional deflections of FGM square ($b = a$) plates resting on a viscoelastic foundation and under hygro-thermo-mechanical loading ($q_0 = 100$, $t_1=0$, $c_1=0$)

P	k_w	k_{p1}	t_2	c_2	$a/h = 5$				$a/h = 10$				$a/h = 20$			
					$\overline{c_t}$				$\overline{c_t}$				$\overline{c_t}$			
					0.05		0.1		0.05		0.1		0.05		0.1	
					Mudhaffar *et al.* (2021)	Present	Mudhaffar *et al.* (2021)	Present	Mudhaffar *et al.* (2021)	Present	Mudhaffar *et al.* (2021)	Present	Mudhaffar *et al.* (2021)	Present	Mudhaffar *et al.* (2021)	Present
0	100	0	0	0	0.2268	0.2287	0.2146	0.2164	0.2028	0.2033	0.1930	0.1935	0.1965	0.1966	0.1873	0.1874
			10	100	1.7290	1.7334	1.6362	0.2820	0.5941	0.5962	0.5654	0.5673	0.2815	0.2959	0.2953	0.2820
	0	100	0	0	0.0432	0.0432	0.0427	0.0428	0.0422	0.0422	0.0418	0.0418	0.0420	0.0419	0.0415	0.0415
			10	100	0.3293	0.3279	0.3258	0.3244	0.1238	0.1239	0.1225	0.1226	0.0631	0.0631	0.0624	0.0625
	100	100	0	0	0.0414	0.0414	0.0410	0.0410	0.0405	0.0405	0.0401	0.0401	0.0403	0.0402	0.0399	0.0398
			10	100	0.3157	0.3143	0.3124	0.3110	0.1187	0.1189	0.1176	0.1177	0.0605	0.0606	0.0599	0.0600
1	100	0	0	0	0.2724	0.2744	0.2550	0.2568	0.2462	0.2467	0.2319	0.2324	0.2392	0.2393	0.2257	0.2258
			10	100	1.9441	2.2425	1.8202	2.0985	0.6850	0.7647	0.6453	0.7202	0.3503	0.3705	0.3305	0.3496
	0	100	0	0	0.0446	0.0446	0.0441	0.0441	0.0439	0.0438	0.0434	0.0433	0.0436	0.0436	0.0432	0.0431
			10	100	0.3185	0.3650	0.3150	0.3610	0.1220	0.1359	0.1207	0.1345	0.0639	0.0675	0.0632	0.0668
	100	100	0	0	0.0427	0.0427	0.0423	0.0423	0.0420	0.0420	0.0416	0.0415	0.0418	0.0418	0.0414	0.0413
			10	100	0.3049	0.3494	0.3017	0.3457	0.1169	0.1302	0.1157	0.1289	0.0612	0.0647	0.0606	0.0640
2	100	0	0	0	0.2855	0.2877	0.2665	0.2684	0.2573	0.2579	0.2418	0.2423	0.2498	0.2499	0.2351	0.2352
			10	100	1.9736	2.3256	1.8421	2.1695	0.7029	0.7970	0.6604	0.7487	0.3627	0.3866	0.3414	0.3639
	0	100	0	0	0.0450	0.0450	0.0445	0.0445	0.0442	0.0442	0.0437	0.0437	0.0440	0.0439	0.0435	0.0434
			10	100	0.3108	0.3638	0.3073	0.3597	0.1207	0.1366	0.1194	0.1351	0.0639	0.0680	0.0632	0.0672
	100	100	0	0	0.0430	0.0430	0.0426	0.0426	0.0423	0.0423	0.0419	0.0419	0.0421	0.0421	0.0417	0.0416
			10	100	0.2974	0.3481	0.2942	0.3444	0.1156	0.1308	0.1144	0.1294	0.0612	0.0651	0.0605	0.0644
5	100	0	0	0	0.2989	0.3012	0.2781	0.2801	0.2682	0.2688	0.2514	0.2519	0.2600	0.2601	0.2441	0.2442
			10	100	2.0090	2.4204	1.8693	2.2509	0.7225	0.8330	0.6771	0.7805	0.3753	0.4034	0.3524	0.3788
	0	100	0	0	0.0453	0.0453	0.0448	0.0448	0.0445	0.0445	0.0440	0.0440	0.0443	0.0442	0.0438	0.0437
			10	100	0.3044	0.3642	0.3010	0.3601	0.1199	0.1379	0.1186	0.1364	0.0639	0.0686	0.0632	0.0679
	100	100	0	0	0.0433	0.0433	0.0429	0.0429	0.0426	0.0426	0.0422	0.0421	0.0424	0.0424	0.0420	0.0419
			10	100	0.2912	0.3484	0.2881	0.3447	0.1148	0.1320	0.1136	0.1306	0.0612	0.0657	0.0606	0.0650

$$\bar{z} = z / h \tag{25}$$

5. Results and discussion

This section presents and analyzes multiple numerical examples aimed at examining the bending behaviors of simply supported FG plates supported by three-parameter elastic foundations. The proposed model is compared against these examples. The composition of the plate is presumed to consist of Titanium and Zirconia, drawing upon the material characteristics detailed by Mudhaffar *et al.* (2021).

Ceramic (Zirconia, ZrO_2): $E_1 = 117.0$ GPa, $\nu = 1/3$, $\alpha_1 = 7.11 \times (10^{-6}/°C)$, $\beta_1 = 0$.

Metal (Titanium, Ti-6Al-4V): $E_2 = 66.2$ GPa, $\nu = 1/3$, $\alpha_2 = 10.3 \times (10^{-6}/°C)$, $\beta_2 = 0.33$

The reference temperature and moisture concentration are set at room temperature $T_0 = 25\,°\text{C}$ and $C_0 = 0\%$. It is assumed, unless stated otherwise, that the pressure is $q_0 = 100$ GPa, $a/h = 10$, $t_1 = 0$, $c_1 = 0$. Numerical results are presented in terms of dimensionless stresses and deflection. The different dimensionless parameters used are

$$\bar{w} = \frac{10^2 h}{a^2 q_0} w\left(\frac{a}{2}, \frac{b}{2}\right), \bar{\sigma}_x = \frac{-10h^2}{a^2 q_0} \sigma_x\left(\frac{a}{2}, \frac{b}{2}, \frac{h}{2}\right),$$

$$\bar{\tau}_{xy} = \frac{10^2 h^2 b}{a^3 q_0} \tau_{xy}\left(0,0,\frac{-h}{2}\right) \bar{\tau}_{xz} = \frac{10hb}{a^2 q_0} \tau_{xz}\left(0,\frac{b}{2},0\right)$$

$$, \bar{k}_w = \frac{k_w a^4}{D_0} \bar{k}_p = \frac{k_p a^2}{D_0} \quad C_T = \frac{c_t a^4}{10^3 D_0} D_0 = \frac{E_b h^3}{12(1-\nu^2)}$$

Table 1 delineates the quantitative findings obtained from the four-variable first order theory employed in this investigation, elucidating the correlation between the current theoretical framework and various advanced shear

Table 3 non-dimensional deflections and stresses of FGM rectangular plates (b/a= 3) subjected to pure mechanical load and resting on a visco-elastic foundation. (a/h=10, q_0=100, t_1=t_2=0, c_1=c_2=0, $k_w = 100, k_p = 100$)

P	C_T	Theory	$\overline{w}$	$\overline{\sigma_x}$	$\overline{\tau}_{xy}$	$\overline{\tau}_{xz}$
0	0	CPT Mudhaffar *et al*. (2021)	0.08201	0.05035	0.07193	–
		Mindlin (1989)	0.08228	0.04890	0.06986	0.03293
		Reddy (2000)	0.08228	0.04919	0.06972	0.04116
		Mudhaffar *et al.* (2021)	0.08226	0.04920	0.07009	0.04356
		Present	0.0823	0.0488	0.0698	-0.0430
	0.05	Mudhaffar *et al.* (2021)	0.08061	0.04821	0.06867	0.04268
		Present	0.0806	0.04786	0.06837	-0.04217
	0.1	Mudhaffar et al.(2021)	0.07901	0.04726	0.06732	0.04184
		Present	0.07902	0.04691	0.06702	-0.04134
	1	Mudhaffar *et al.* (2021)	0.05829	0.03486	0.04966	0.03087
		Present	0.05829	0.03460	0.04943	-0.03049
1	0	CPT Mudhaffar *et al*. (2021)	0.08399	0.04683	0.05353	–
		Mindlin (1989)	0.08418	0.04546	0.05198	0.02572
		Reddy (2000)	0.08417	0.04574	0.05190	0.03214
		Mudhaffar *et al*. (2021)	0.08417	0.04575	0.05217	0.03403
		Present	0.08418	0.04539	0.05192	-0.03362
	0.05	Mudhaffar *et al*. (2021)	0.08244	0.04480	0.05109	0.03333
		Present	0.08244	0.04445	0.05085	-0.03293
	0.1	Mudhaffar *et al*. (2021)	0.08077	0.04390	0.05006	0.03265
		Present	0.08078	0.04356	0.04982	-0.03226
	1	Mudhaffar *et al.* (2021)	0.05924	0.03220	0.03672	0.02395
		Present	0.05924	0.03194	0.03654	-0.02366
2	0	CPT Mudhaffar *et al.* (2021)	0.08437	0.04655	0.04931	–
		Mindlin (1989)	0.08457	0.04515	0.04781	0.02303
		Reddy (2000)	0.08457	0.04539	0.04770	0.02951
		Mudhaffar *et al.* (2021)	0.08456	0.04541	0.04794	0.03131
		Present	0.08457	0.04504	0.04772	-0.03076
	0.05	Mudhaffar *et al.* (2021)	0.08281	0.04447	0.04695	0.03066
		Present	0.08281	0.04411	0.04673	-0.03012
	0.1	Mudhaffar *et al*. (2021)	0.08113	0.04357	0.04600	0.03004
		Present	0.08113	0.04321	0.04579	-0.02951
	1	Mudhaffar *et al*. (2021)	0.05943	0.03192	0.03370	0.02201
		Present	0.05943	0.03165	0.03354	-0.02162
5	0	CPT Mudhaffar *et al.* (2021)	0.08471	0.04780	0.04714	–
		Mindlin (1989)	0.08491	0.04630	0.04568	0.02085
		Reddy (2000)	0.08491	0.04652	0.04549	0.02735
		Mudhaffar *et al*. (2021)	0.08491	0.04655	0.04574	0.02910
		Present	0.08491	0.04616	0.04553	-0.02845
	0.05	Mudhaffar *et al*. (2021)	0.08314	0.04558	0.04479	0.02849
		Present	0.08315	0.04520	0.04459	-0.02786
	0.1	Mudhaffar *et al*. (2021)	0.08145	0.04465	0.04388	0.02791
		Present	0.08146	0.04428	0.04368	-0.02729
	1	Mudhaffar *et al*. (2021)	0.05960	0.03268	0.03211	0.02043
		Present	0.05960	0.03240	0.03196	-0.01997

deformation theories. Furthermore, the impact of the volume fraction exponent ratio (p) alongside the effect of an elastic foundation on the dimensionless deflection characteristics of functionally graded material (FGM)

Table 4 Influence of gradient index on non-dimensional deflections and stresses of FGM rectangular plates (b/a= 3) resting on a viscoelastic foundation and under linear hygro-thermo-mechanical load. (a/h=10,q_0=100,t_1= 0,t_2=10,c_1 =0,c_2=100)

P	C_T	Theory	$\overline{w}$	$\overline{\sigma_x}$	$\overline{\tau}_{xy}$	$\overline{\tau}_{xz}$
0	0	Mudhaffar *et al.* (2021)	0.17266	-0.50297	0.17581	-0.40819
		Present	0.1730	-0.5018	0.1744	0.4056
	0.05	Mudhaffar *et al.* (2021)	0.16918	-0.50505	0.17285	-0.41004
		Present	0.1695	-0.5039	0.1714	0.4074
	0.1	Mudhaffar *et al.* (2021)	0.16584	-0.50705	0.17000	-0.41181
		Present	0.1661	-0.5059	0.1686	0.4091
	1	Mudhaffar *et al.* (2021)	0.12234	-0.53307	0.13294	−0.43484
		Present	0.1226	-0.5318	0.1316	0.4319
1	0	Mudhaffar et al.(2021)	0.18457	-0.51268	0.15698	-0.46946
		Present	0.1849	-0.5099	0.1559	0.4646
	0.05	Mudhaffar *et al.* (2021)	0.18076	-0.51475	0.15462	-0.47099
		Present	0.1811	-0.5120	0.1535	0.4661
	0.1	Mudhaffar *et al.* (2021)	0.17711	-0.51673	0.15236	-0.47247
		Present	0.1774	-0.5140	0.1513	0.4676
	1	Mudhaffar *et al.* (2021)	0.12990	-0.54239	0.12310	-0.49156
		Present	0.1301	-0.5395	0.1221	0.4865
2	0	Mudhaffar *et al.* (2021)	0.18511	-0.50165	0.13522	-0.46362
		Present	0.1855	-0.4984	0.1339	0.4535
	0.05	Mudhaffar *et al.* (2021)	0.18128	-0.50371	0.13305	-0.46504
		Present	0.1816	-0.5005	0.1318	0.4549
	0.1	Mudhaffar *et al.* (2021)	0.17760	-0.50569	0.13096	-0.46640
		Present	0.1780	-0.5024	0.1297	0.4563
	1	Mudhaffar *et al.* (2021)	0.13010	-0.53120	0.10403	-0.48399
		Present	0.1304	-0.5278	0.1028	0.4736
5	0	Mudhaffar *et al.* (2021)	0.18646	-0.48782	0.12494	-0.46400
		Present	0.1868	-0.4838	0.1234	0.4500
	0.05	Mudhaffar *et al.* (2021)	0.18259	-0.48994	0.12285	-0.46661
		Present	0.1829	-0.4859	0.1213	0.4513
	0.1	Mudhaffar *et al.* (2021)	0.17887	-0.49198	0.12085	-0.48305
		Present	0.1792	-0.4879	0.1193	0.4525
	1	Mudhaffar *et al.* (2021)	0.13089	-0.51829	0.09501	-0.45993
		Present	0.1311	-0.5141	0.0935	0.4686

rectangular plates is examined comprehensively, taking into account the influences of temperature and humidity. The findings are juxtaposed with those forecasted by Sayyad and Ghugal (2019).

The number of primary variables in this improved theory is lower compared to other higher-order shear deformation plate theories. this theory provides a better understanding of the hygro-thermo-mechanical behavior of the materials and structures under study. This new approach aims to address some of the limitations of the conventional FSDT, offering more accurate results while simplifying certain aspects of the calculating process. In conclusion, The theory put forward is not only precise but also fairly simple, establishing itself as an essential resource for anticipating the hygro-thermo-mechanical bending responses of functionally graded material (FGM) plates resting on Winkler or Pasternak elastic foundations.

Table 2 compellingly demonstrates how sinusoidal loads influence the central nondimensional deflection of a square functionally graded material (FGM) plate that is supported by a viscoelastic foundation, while varying the material gradient index (p). This insight is crucial for understanding the performance and stability of such plates under different loading conditions. The results reveal that the Winkler viscoelastic foundation results in higher deflection compared to the Pasternak foundation. Moreover, the deflection is greater when the plate is exposed to hygro-thermal loads than under purely mechanical loading. It is also observed that increasing the damping coefficient $C_T$of the viscoelastic foundation reduces the deflection. For all types of loading, the deflection noticeably decreases as the damping effect increases. Additionally, as the gradient index rises—thereby reducing the plate's stiffness—Under

Table 5 Influence of porosity on the non-dimensional deflections of FGM square ($b = a$) plates resting on a viscoelastic foundation and under hygro-thermo-mechanical loading.(q_0 = 100, t_1=0,c_1=0 ,C_T=0.1)

P	k_w	k_{p1}	t_2	c_2	$a/h = 5$				$a/h = 10$				$a/h = 20$			
					xi				XI				XI			
					0	0.1	0.2	0.3	0	0.1	0.2	0.3	0	0.1	0.2	0.3
0	100	0	0	0	0.2164	0.2284	0.2420	0.2572	0.1935	0.2049	0.2177	0.2322	0.1974	0.1986	0.2112	0.2254
			10	100	1.6397	1.4118	1.1934	0.9860	0.5673	0.5166	0.4691	0.4255	0.2821	0.2776	0.2749	0.2745
	0	100	0	0	0.0428	0.0433	0.0437	0.0442	0.0418	0.0423	0.0429	0.0434	0.0415	0.0421	0.0426	0.0432
			10	100	0.3244	0.2674	0.2157	0.1695	0.1227	0.1068	0.0924	0.0795	0.0625	0.0588	0.0555	0.0525
	100	100	0	0	0.0411	0.0415	0.0419	0.0423	0.0402	0.0406	0.0411	0.0416	0.0399	0.0404	0.0409	0.0414
			10	100	0.3111	0.2563	0.2066	0.1623	0.1177	0.1024	0.0886	0.0762	0.0600	0.0564	0.0532	0.0504
1	100	0	0	0	0.2568	0.2745	0.2948	0.3186	0.2324	0.2495	0.2695	0.2931	0.2258	0.2428	0.2626	0.2862
			10	100	2.0986	1.8514	1.6126	1.3842	0.7203	0.6688	0.6214	0.5790	0.3497	0.3493	0.3521	0.3590
	0	100	0	0	0.0442	0.0447	0.0452	0.0457	0.0434	0.0440	0.0445	0.0452	0.0432	0.0438	0.0444	0.0450
			10	100	0.3610	0.3014	0.2472	0.1986	0.1345	0.1178	0.1027	0.0898	0.0668	0.0629	0.0595	0.0564
	100	100	0	0	0.0423	0.0428	0.0432	0.0437	0.0416	0.0421	0.0426	0.0432	0.0414	0.0419	0.0425	0.0430
			10	100	0.3458	0.2885	0.2365	0.1899	0.1289	0.1129	0.0983	0.0853	0.0641	0.0631	0.0569	0.0540
2	100	0	0	0	0.2684	0.2879	0.3105	0.3373	0.2423	0.2611	0.2832	0.3098	0.2352	0.2538	0.2757	0.3022
			10	100	2.1695	1.9165	1.6714	1.4361	0.7488	0.6970	0.6495	0.6074	0.3640	0.3647	0.3691	0.3782
	0	100	0	0	0.0445	0.0450	0.0455	0.0461	0.0437	0.0443	0.0449	0.0455	0.0435	0.0441	0.0448	0.0454
			10	100	0.3598	0.2997	0.2452	0.1962	0.1351	0.1183	0.1030	0.0893	0.0673	0.0634	0.0599	0.0568
	100	100	0	0	0.0426	0.0431	0.0436	0.0441	0.0419	0.0424	0.0430	0.0435	0.0417	0.0422	0.0428	0.0434
			10	100	0.3445	0.2868	0.2345	0.1875	0.1295	0.1133	0.0986	0.0854	0.0645	0.0607	0.0573	0.0543
5	100	0	0	0	0.2802	0.3012	0.3258	0.3550	0.2520	0.2721	0.2958	0.3247	0.2442	0.2640	0.2875	0.3159
			10	100	2.2509	1.9911	1.7386	1.4952	0.7806	0.7282	0.6800	0.6375	0.3789	0.3804	0.3857	0.3961
	0	100	0	0	0.0448	0.0453	0.0459	0.0464	0.0440	0.0446	0.0452	0.0458	0.0438	0.0444	0.0450	0.0457
			10	100	0.3602	0.2997	0.2447	0.1954	0.1365	0.1194	0.1039	0.0900	0.0679	0.0640	0.0604	0.0572
	100	100	0	0	0.0429	0.0437	0.0438	0.0443	0.0422	0.0427	0.0433	0.0438	0.0420	0.0425	0.0431	0.0437
			10	100	0.3447	0.2867	0.2340	0.1867	0.1307	0.1143	0.0994	0.0861	0.0651	0.0612	0.0578	0.0547

the same loading conditions, deflection decreases with an increase in the plate's geometric ratio (a/h), and the influence of the viscoelastic foundation is more significant for thicker plates.

Table 3 examines how the gradient index (p) affects the deflection and stresses in an FGM plate under pure bending, while keeping the Winkler and Pasternak coefficientsunchanged. When the viscoelastic foundation damping is set to zero, the deflection results align well with both classical plate theory and previous literature, as shown in the Table 3. Increasing the gradient index leads to a higher central deflection and a reduction in both longitudinal and shear stresses. Furthermore, increasing the viscoelastic damping coefficient (C_T) results in significant reductions in both deflection and stresses, demonstrating the crucial role the viscoelastic foundation plays in the plate's design performance.

Table 4 shows the effect of linear hygro-thermal loads combined with mechanical loading on a rectangular FGM plate supported by a viscoelastic foundation. The deflection and stresses are higher compared to the case of pure bending presented in Table 4. This indicates that environmental factors impact the material's durability as well as the induced stresses and deflection. Additionally, it is observed that as the material index p increases, the deflection increases while the stresses decrease. Furthermore, increasing the damping coefficient of the viscoelastic foundation reduces both deflection and stresses, as illustrated in Fig. 2.

The influence of porosity on the non-dimensional deflections of functionally graded material (FGM) square plates on a viscoelastic foundation under combined hygro-thermo-mechanical loading is discussed in this section. Table 5 illustrates the impact of xi, thermal and moisture loads, k_w and k_p on non-dimensional deflections of FG porous plate. As moisture and thermal parameters increase, so does $\overline{w}$, while higher Winkler Pasternack foundation parameter lead to a decrease. Moving on to Table 6, the effects of p, xi on the displacement and stresses of FG non-porous and porous plate under linear hygro-thermo-mechanical load are displayed. The stresses induced by FG porous plate are notably lower compared to FG non-porous plate. Additionally, higher xi contributes to greater $\overline{w}$ due to increased moisture absorption, and higher thermal loads result in increased $\overline{w}$. Stresses in FG porous plate are generally lower than FG non-porous plate due to pore presence. Furthermore, higher p and xi lead to decreased stresses. The interplay of these factors determines stress distribution and magnitude in the plate. This comprehensive analysis underscores the influences of various factors on.

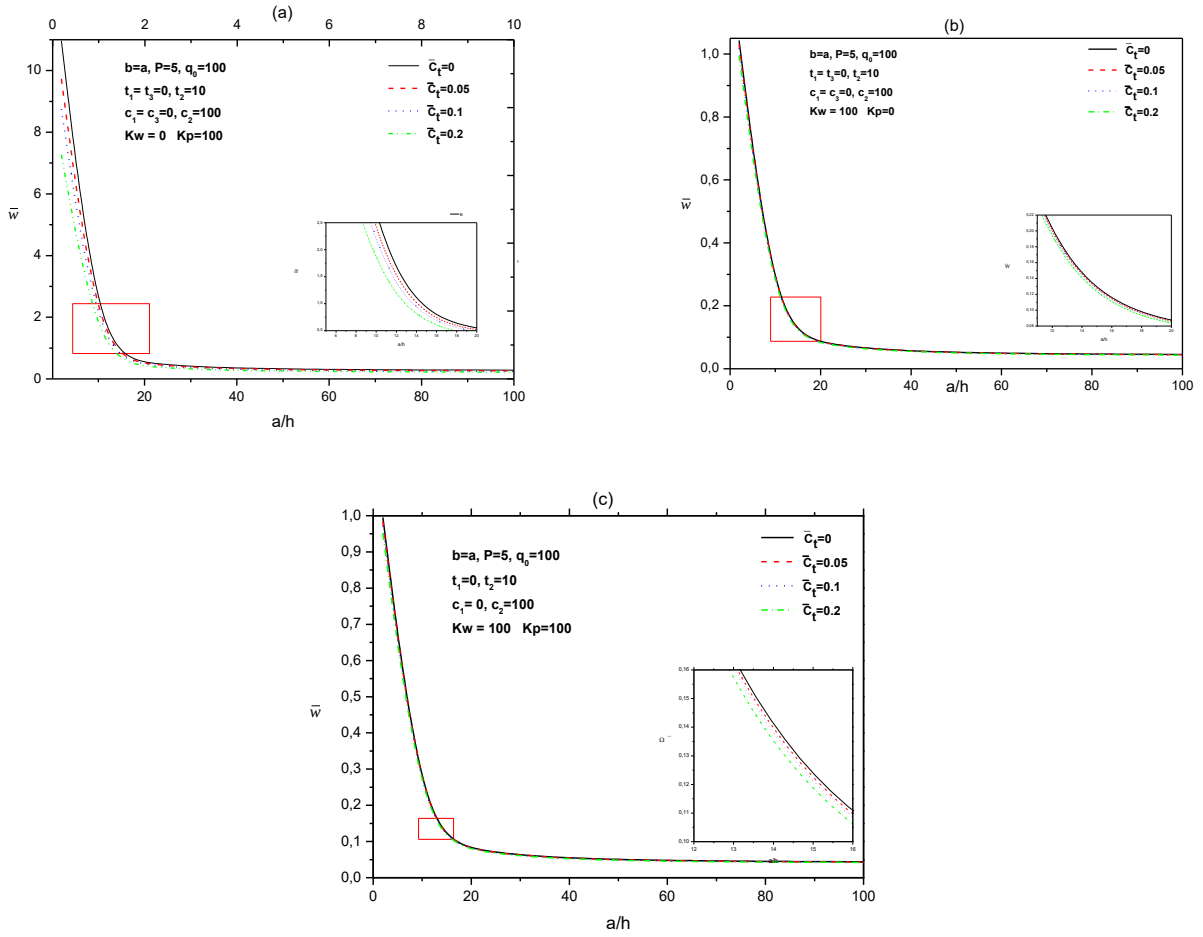

Fig. 2 Aspect ratio (a/h) influence on the non-dimensional deflection of FGM square plate under linear hygro-thermo-mechanical load and resting on a viscoelastic foundation $\bar{w}$

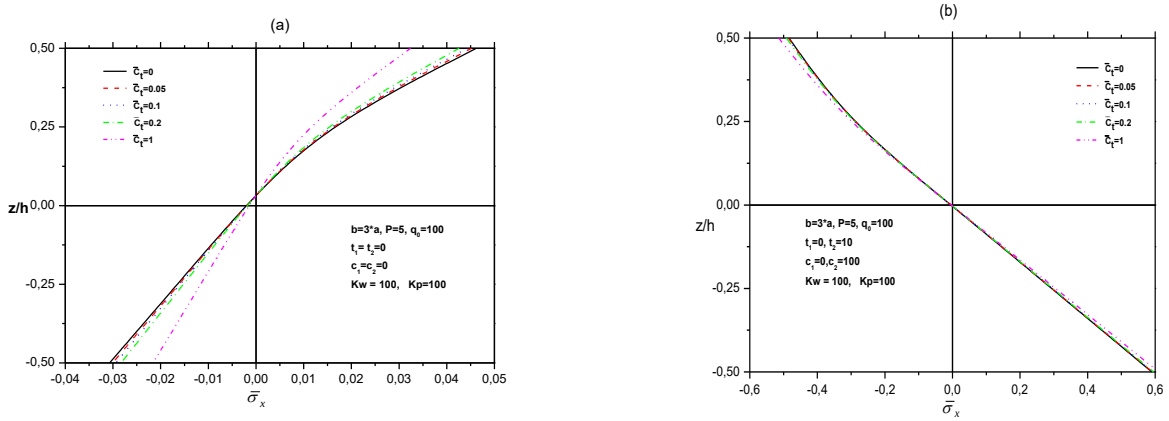

Fig. 3 Non-dimensional variation of in-plane normal stress $\bar{\sigma}_x$ across the thickness of FGM rectangular plate resting on viscoelastic foundation

deflection and stresses, emphasizing the complex behavior of FG porous plates under different conditions

Fig. 3 illustrates the significant variation of normal stress values within the plate, clearly indicating a transition from distinctly negative values present at the lower region of the plate to notably positive values encountered at the upper region. Fig. 4 conducts an in-depth analysis of how the viscoelastic foundation damping coefficient significantly influences the distribution patterns of the non-dimensional in-plane shear stress throughout the thickness

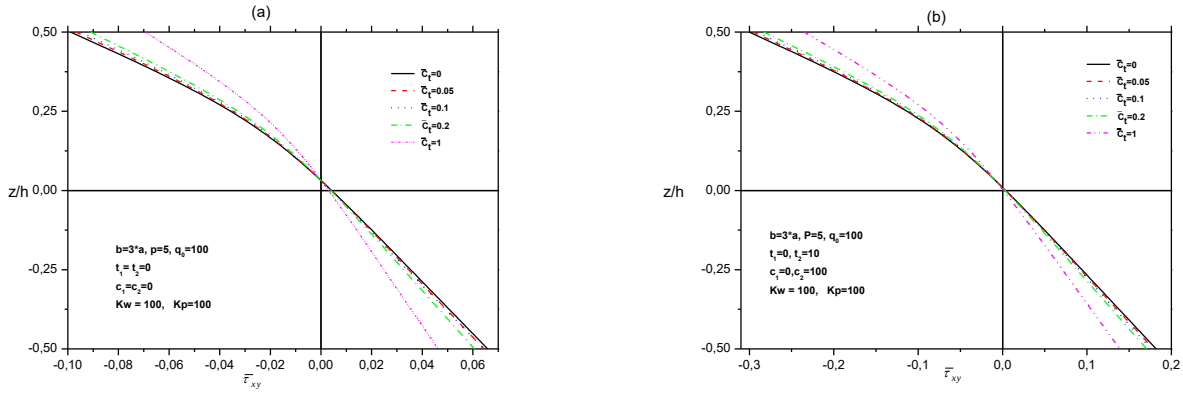

Fig. 4 Non-dimensional variation of $\overline{\tau}_{xy}$ across the thickness of FGM rectangular plate resting on a viscoelastic foundation

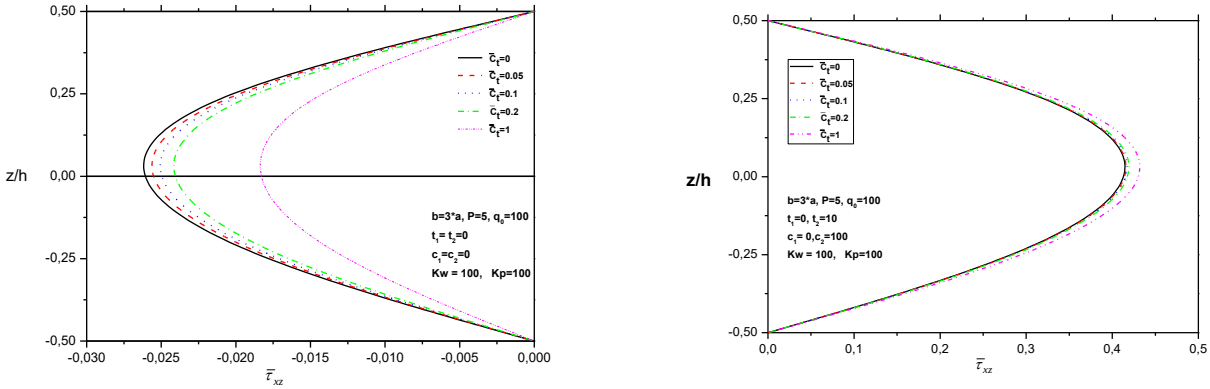

Fig. 5 Non-dimensional variation of transverse shear stress $\overline{\tau}_{xz}$ across the thickness of FGM rectangular plate resting on a viscoelastic foundation

Table 6 Influence of porosity on non-dimensional deflections and stresses of FGM rectangular plates (b/a = 3) resting on a viscoelastic foundation and under linear hygro-thermo-mechanical load. (a/h = 10, q_0 = 100, t_1 = 0, t_2 = 10, c_1 = 0, c_2 = 100, $k_w = 100$ $k_p = 100$)

P	XI	$\overline{w}$	$\overline{\sigma_x}$	$\overline{\tau}_{xy}$	$\overline{\tau}_{xz}$
0	0	0.1661	-0.5059	0.1686	0.4091
	0.1	0.1487	-0.3947	0.1381	0.3189
	0.2	0.1330	-0.2947	0.1117	0.2378
	0.3	0.1191	-0.2063	0.0892	0.1660
1	0	0.1774	-0.5140	0.1513	0.4676
	0.1	0.1593	-0.4026	0.1217	0.3741
	0.2	0.1430	-0.3025	0.0960	0.2898
	0.3	0.1286	-0.2140	0.0739	0.2150
2	0	0.1779	-0.5024	0.1297	0.4563
	0.1	0.1597	-0.3911	0.1011	0.3633
	0.2	0.1432	-0.2910	0.0764	0.2796
	0.3	0.1286	-0.2023	0.0553	0.2054
5	0	0.1792	-0.4880	0.1193	0.4525
	0.1	0.1608	-0.3772	0.0915	0.3593
	0.2	0.1442	-0.2776	0.0675	0.2755
	0.3	0.1294	-0.1892	0.0471	0.2011

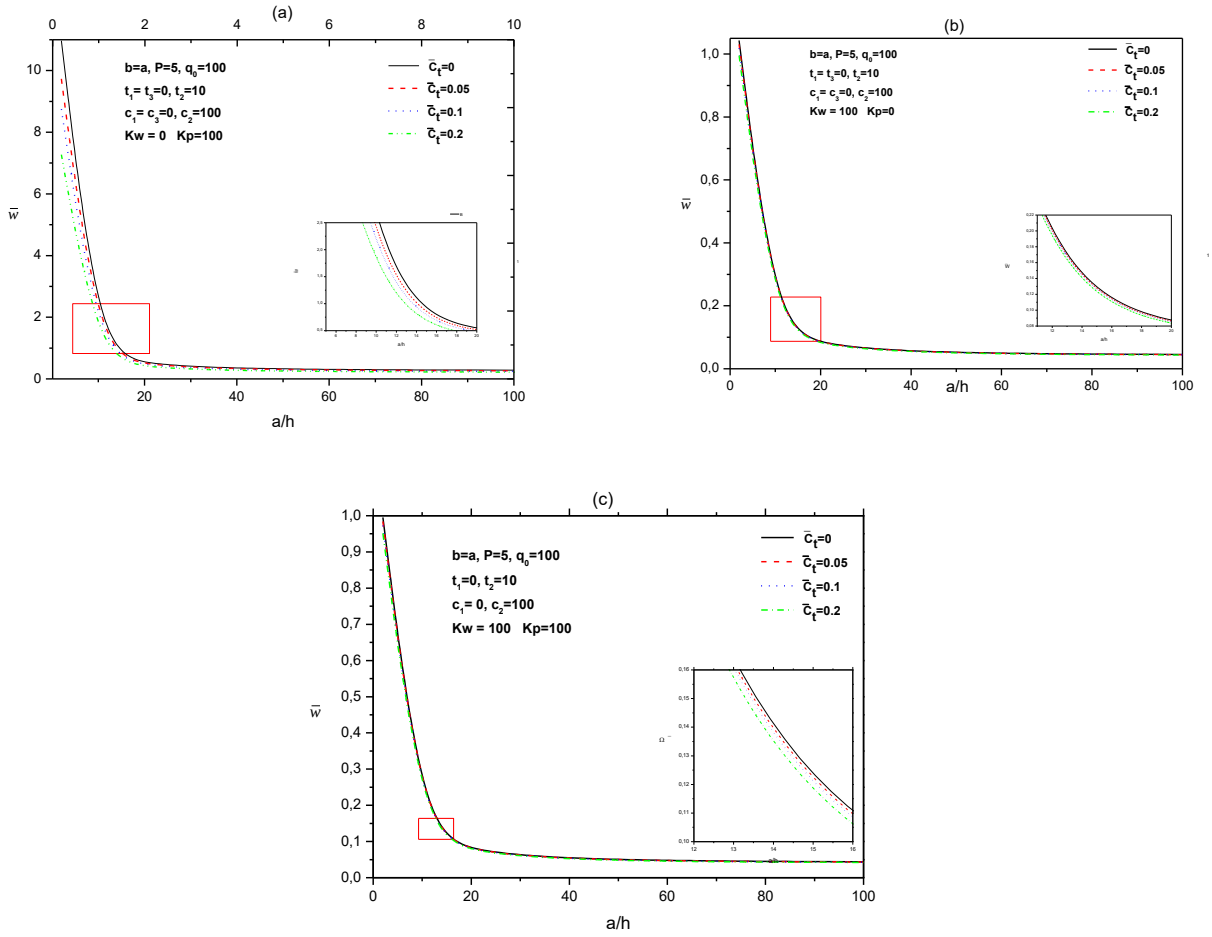

Fig. 6 Aspect ratio (a/h) influence on the non-dimensional deflection $\bar{w}$ of FGM square plate under linear hygro-thermo-mechanical load and resting on a viscoelastic foundation

of the functionally graded (FG) plate. It is observed that $\bar{\tau}_{xy}$ reaches its peak values at both the top and bottom surfaces of the plate, showcasing the critical regions where stress concentration occurs. In Fig. 5, the detailed analysis of the transverse shear stress $\bar{\tau}_{xz}$ reveals that its maximum value occurs right at the center of the plate, while it interestingly remains zero at both the upper and lower surfaces. This characteristic behavior is achieved without the necessity of a shear correction factor, which effectively highlights a key advantage afforded by the present shear deformation theory. Furthermore, the data suggest that an increase in the damping coefficient (C_T) leads to a notable decrease in the transverse shear stress experienced by the plate, reinforcing the relationship between material properties and stress distributions under varying conditions.

6. Conclusions

This research investigated the bending response under combined hygro-thermo-mechanical conditions of advanced functionally graded ceramic-metal plates, which were supported by a viscoelastic foundation characterized by three parameters. The analysis employed a straightforward first-order shear deformation theory. An analytical solution was obtained using the Navier method. Notable influences of temperature and moisture content were identified. Furthermore, the role of the viscoelastic foundation on plate deflection and stress levels was deemed critical. The incorporation of the viscoelastic foundation markedly decreases the central deflection. The parametric analysis highlighted the overall influence of various parameters such as pore distribution, material grading, and loading conditions on the mechanical performance of these structures. This study aims to elucidate the complex interplay between these factors and their collective impact on the structural integrity of graded plates. various factors on the bending response of functionally graded materials (FGM) plates. Across all loading conditions, an increase in the viscous damping coefficient leads to a reduction in deflection. Ultimately, the conclusions drawn from this article aim to improve the design efficiency of advanced FGM plates by taking into account the effects of these factors. An important advantage of the proposed methodology lies in its balance between simplicity and accuracy. By reducing the number of displacement variables without compromising the quality of results, the model offers an efficient yet reliable tool for analyzing complex environmental and structural interactions. The analytical solution obtained via the Navier method ensures

both precision and computational efficiency, making it well-suited for practical applications in aerospace, mechanical, civil, and marine engineering, where lightweight and thermally stable structural components are essential. Additionally, future research will focus on optimizing the design parameters to enhance the performance of functionally graded material sandwich plates in practical applications (Amiri *et al*. 2024, Alimoradzadeh and Akbas 2023, Adim and Daouadji 2024, Turan 2024).

Acknowledgements

The authors extend their appreciation to Taif University, Saudi Arabia, for supporting this work through project number (TU-DSPP-2024-66).

References

Adim, B. and Daouadji, T.H. (2016), "Effects of thickness stretching in FGM plates using a quasi-3D higher order shear deformation theory", *Adv. Mater. Res.*, **5**(4), 223-244. https://doi.org/10.12989/amr.2016.5.4.223.

Adim, B. and Daouadji, T.H. (2024), "Analysis of the hygro-thermo-mechanical response of functionally graded plates resting on elastic foundations based on various micromechanical models", *Geomech. Eng.*, **38**(4), 409-420. https://doi.org/10.12989/gae.2024.38.4.409.

Ahmed, R.A., Khalaf, B.S., Raheef, K.M., Fenjan, R.M. and Faleh, N.M. (2021), "Investigating dynamic response of nonlocal functionally graded porous piezoelectric plates in thermal environment", *Steel Compos. Struct.*, **40**(2), 243-254. https://doi.org/10.12989/scs.2021.40.2.243.

Ahmed, R.A., Al-Maliki, A.F. and Faleh, N.M. (2020), "Dynamic characteristics of multi-phase crystalline porous shells with using strain gradient elasticity", *Adv. Nano Res.*, **8**(2), 157-167. https://doi.org/10.12989/anr.2020.8.2.157.

Ahmed, R.A., Fenjan, R.M. and Faleh, N.M. (2019), "Analyzing post-buckling behavior of continuously graded FG nanobeams with geometrical imperfections", *Geomech. Eng.*, **17**(2), 175-180. https://doi.org/10.12989/gae.2019.17.2.175.

Akbaş, Ş.D. (2021), "Dynamic analysis of axially functionally graded porous beams under a moving load", *Steel Compos. Struct.*, **39**(6), 811-821. https://doi.org/10.12989/scs.2021.39.6.811.

Alimoradzadeh, M. and Akbas, S.D. (2023), "Nonlinear vibration analysis of carbon nanotube-reinforced composite beams resting on nonlinear viscoelastic foundation", *Geomech. Eng.*, **32**(2), 125-135.https://doi.org/10.12989/gae.2023.32.2.125.

Al-Toki, M.H., Fenjan, R.M., Ahmed, R.A., Faleh, N.M. and Abdullah, W.N. (2021), "Analyzing dynamic characteristics of nonlocal porous graded beams under impulse and thermal loading", *Adv. Comput. Des.*, **6**(4), 301-317. https://doi.org/10.12989/acd.2021.6.4.361.

Amiri, M., Loghman, A. and Arefi, M. (2022), « Thermoelastic analysis of rectangular plates with variable thickness made of FGM based on TSDT using DQ method", *Geomech. Eng.*, **29**(6), 667-681. https://doi.org/10.12989/gae.2022.29.6.667.

Arefi, M. and Meskini, M. (2019), "Application of hyperbolic shear deformation theory to free vibration analysis of functionally graded porous plate with piezoelectric face-sheets", *Struct. Eng. Mech.*, **71**(5), 459-467. https://doi.org/10.12989/sem.2019.71.5.459.

Arshid, E. and Khorshidvand, A.R. (2018), "Free vibration analysis of saturated porous FG circular plates integrated with piezoelectric actuators via differential quadrature method", *Thin-Wall. Struct.*, **125**, 220-233. http://doi.org/10.1016/j.tws.2018.01.007.

Avcar, M. (2019), "Free vibration of imperfect sigmoid and power law functionally graded beams", *Steel Compos. Struct.*, **30**(6), 603-615. https://doi.org/10.12989/scs.2019.30.6.603.

Barati, M.R. (2018), "A general nonlocal stress-strain gradient theory for forced vibration analysis of heterogeneous porous nanoplates", *Eur. J. Mech. A Solids*, **67**, 215-230. https://doi.org/10.1016/j.euromechsol.2017.09.001.

Baseri, V., Jafari, G.S. and Kolahchi, R. (2016), "Analytical solution for buckling of embedded laminated plates based on higher order shear deformation plate theory", *Steel Compos. Struct.*, **21**(4), 883-919. https://doi.org/10.12989/scs.2016.21.4.883.

Beg, M.S., Khalid, H.M., Yasin, M.Y. and Hadji, L. (2021), "Exact third-order static and free vibration analyses of functionally graded porous curved beam", *Steel Compos. Struct.*, **39**(1), 1-20. https://doi.org/10.12989/scs.2021.39.1.001.

Benkhedda, A., Tounsi, A. and Adda bedia, E.A. (2008), "Effect of temperature and humidity on transient hygrothermal stresses during moisture desorption in laminated composite plates", *Compos. Struct.*, **82**(4), 629-635. https://doi.org/10.1016/j.compstruct.2007.04.013.

Birman, V. and Byrd, L.W. (2007) , "Modeling and analysis of functionally graded materials and structures", **60**(5), 195-216. https://doi.org/10.1115/1.2777164

Bot, I.K., Bousahla, A.A., Zemri, A., Sekkal, M., Kaci, A., Bourada, F., Tounsi, A., Ghazwani, M.H. and Mahmoud, S.R. (2022), "Effects of Pasternak foundation on the bending behavior of FG porous plates in hygrothermal environment", *Steel Compos. Struct.*, **43**(6), 821-837. https://doi.org/10.12989/scs.2022.43.6.821.

Çapar, Ö.F., Çalım, M.H., Özbey, M.B. and Cuma, Y.C. (2024), "Dynamic analysis of viscoelastic porous functionally graded plates resting on elastic foundation", **39**(3), 257-271. https://doi.org/10.12989/gae.2024.39.3.257.

Carrera, E., Brischetto, S. and Robaldo, A. (2008), "Variable kinematic model for the analysis of functionally graded material plates", *AIAA J.*, **46**(1), 194-203. https://doi.org/10.2514/1.32490.

Cho, J.R. (2023), "Neutral surface-based static and free vibration analysis of functionally graded porous plates", *Steel Compos. Struct.*, **49**(4), 431-440. https://doi.org/10.12989/scs.2023.49.4.431.

Cinefra, M., Petrolo, M., Li, G. and Carrera, E. (2017), "Hygrothermal analysis of multilayered composite plates by variable kinematic finite elements", *J. Therm. Stresses*, **40**(12), 1502-1522. https://doi.org/10.1080/01495739.2017.1360164.

Cong, P.H., Chien, T.M., Khoa, N.D. and Duc, N.D. (2018), "Nonlinear thermomechanical buckling and post-buckling response of porous FGM plates using Reddy's HSDT", *Aerosp Sci. Technol.*, **77**, 419-428. https://doi.org/10.1016/j.ast.2018.03.020.

Daouadji, T.H. and Benferhat, R. (2016), "Bending analysis of an imperfect FGM plates under hygro-thermo-mechanical loading with analytical validation", *Adv. Mater. Res.*, **5**(1), 35-53. https://doi.org/10.12989/amr.2016.5.1.035.

Ebrahimi, F. and Habibi, S. (2016), "Deflection and vibration analysis of higher-order shear deformable compositionally graded porous plate", *Steel Compos. Struct.*, **20**(1), 205-225. https://doi.org/10.12989/scs.2016.20.1.205.

Ebrahimi, F., Dabbagh, A., Tornabene, F. and Civalek, O. (2019), "Hygro-thermal effects on wave dispersion responses of magnetostrictive sandwich nanoplates", *Adv. Nano Res.*, **7**(3),

157-167. https://doi.org/10.12989/anr.2019.7.3.157.

Ebrahimi, F., Jafari, A. and Selvamani, R. (2020), "Thermal buckling analysis of magneto-electro-elastic porous FG beam in thermal environment", *Adv. Nano Res.*, **8**(1), 83-94. http://dx.doi.org/10.12989/anr.2020.8.1.083.

Feyzi, M.R. and Khorshidvand, A.R. (2017), "Axisymmetric post-buckling behavior of saturated porous circular plates", *Thin-Wall. Struct.*, **112**, 149-158. https://doi.org/10.1016/J.TWS.2016.11.026.

Gupta, A. and Talha, M. (2015), "Recent development in modeling and analysis of functionally graded materials and structures", *Prog. Aerosp. Sci.*, ***79***, 1-14. https://doi.org/10.1016/j.paerosci.2015.07.001.

Hamad, L.B., Khalaf, B.S. and Faleh, N.M. (2019), "Analysis of static and dynamic characteristics of strain gradient shell structures made of porous nano-crystalline materials", *Adv. Mater. Res.*, **8**(3), 179-96. https://doi.org/10.12989/amr.2019.8.3.179.

Hamed, M.A., Abo-Bakr, R.M., Mohamed, S.A. and Eltaher, M.A. (2020), "Influence of axial load function and optimization on static stability of sandwich functionally graded beams with porous core", *Eng. Comput.*, **36**(4), 1929-1946. https://doi.org/10.1007/s00366-020-01023-w.

Huang, W. and Tahouneh, V. (2021), "Frequency study of porous FGPM beam on two-parameter elastic foundations via Timoshenko theory", *Steel Compos. Struct.*, **40**(1), 139-156. https://doi.org/10.12989/scs.2021.40.1.139.

Jain, R. and Azam, M.S. (2024), "Deflection and bending characteristics of embedded functionally graded porous plate with bi-directional thickness variation subjected to bi-sinusoidal loading", *Steel Compos. Struct.*, **51**(6), 601-617. https://doi.org/10.12989/scs.2024.51.6.601.

Keleshteri, M.M. and Jelovica, J. (2021), "Nonlinear vibration analysis of bidirectional porous beams", *Eng. Comput.*, https://doi.org/10.1007/s00366-021-01553-x.

Kerr, A.D. (1964), "Elastic and viscoelastic foundation models," https://doi.org/10.1115/1.3629667

Khider, A.S., Aalsaud, A., Faleh, N.M., Abd, A.K., Al-Jaafari, M.A. and Fenjan, R.M. (2024), "A review on dynamic characteristics of nonlocal porous FG nanobeams under moving loads", *Steel Compos. Struct.*, **50**(1), 15-24. https://doi.org/10.12989/scs.2024.50.1.015.

Khorshidvand, A.R., Farzaneh Joubaneh, E., Jabbari, M. and Eslami, M.R. (2014), "Buckling analysis of a porous circular plate with piezoelectric sensor actuator layers under uniform radial compression", *Acta Mech.*, **225**, 179-193. https://doi.org/10.1007/s00707-013-0959-2.

Kumar, R., Bajaj, M., Singh, J. and Shukla, K.K. (2022c), "New HSDT for free vibration analysis of elastically supported porous bidirectional functionally graded sandwich plate using collocation method", *Proceedings of the Institution of Mechanical Engineers, Part C: Journal of Mechanical Engineering Science*, **236**(16), 9109-9123. https://doi.org/10.1177/09544062221090075.

Kumar, R., Gupta, K.K., Singh, J. and Singh, J. (2023b), "Radial basis collocation method for free vibration analysis of elastically supported porous bi-directional FGM plate under various types of porosity distribution", *Adv. Mater. Process. Technol.*, **9**(2), 368-390. https://doi.org/10.1080/2374068X.2022.2093003.

Kumar, R., Jain, A., Singh, M., Singh, J. and Singh, J. (2023c), "Porosity-dependent buckling analysis of elastically supported FGM sandwich plate via new tangent HSDT: A meshfree approach", *Int. J. Comput. Mater. Sci. Eng.*, **12**(1), 2250013. https://doi.org/10.1142/S2047684122500130.

Kumar, R., Kumar, C., Singh, M., Damania, J., Singh, J. and Singh, J. (2022a), "A meshfree approach for bending analysis of porous rectangular FGM plate resting on elastic foundation", *Mech. Adv. Compos. Struct.*, **9**(2), 303-316. https://doi.org/10.22075/macs.2022.26674.1388.

Kumar, R., Lal, A., Singh, B.N. and Singh, J. (2019a), "Meshfree approach on buckling and free vibration analysis of porous FGM plate with proposed IHHSDT resting on the foundation", *Curved Layered Struct.*, ***6***(1), 192-211. https://doi.org/10.1515/cls-2019-0017.

Kumar, R., Lal, A., Singh, B.N. and Singh, J. (2019b), "New transverse shear deformation theory for bending analysis of FGM plate under patch load", *Compos. Struct.*, **208**, 91-100. https://doi.org/10.1016/j.compstruct.2018.10.014.

Kumar, R., Lal, A., Singh, B.N. and Singh, J. (2022d), "Numerical simulation of the thermomechanical buckling analysis of bidirectional porous functionally graded plate using collocation meshfree method", *Proceedings of the Institution of Mechanical Engineers, Part L: J. Mater. Des. Appl.*, **236**(4), 787-807. https://doi.org/10.1177/14644207211058573.

Kumar, R., Singh, B.N. and Singh, J. (2023a), "Geometrically nonlinear analysis for flexure response of FGM plate under patch load", *Mech. Based Des. Struc.*, **51**(11), 6532-6556. https://doi.org/10.1080/15397734.2022.2058015.

Kumar, R., Singh, B.N., Singh, J. and Singh, J. (2022b), "Meshfree approach for flexure analysis of bidirectional porous FG plate subjected to I, L, and T types of transverse loading", *Aerosp. Sci. Technol.*, **129**, 107824. https://doi.org/10.1016/j.ast.2022.107824.

Leissa, A.W. (1973), "The free vibration of rectangular plates", *J. Sound Vib.*, **31**(3), 257-293. https://doi.org/10.1016/S0022-460X(73)80371-2.

Li, M., Soares, C.G. and Yan, R. (2020), "A novel shear deformation theory for static analysis of functionally graded plates", *Compos. Struct.*, **250**, 112559. https://doi.org/10.1016/j.compstruct.2020.112559.

Lo, S.H., Zhen, W., Cheung, Y.K. and Wanji, C. (2010), "Hygrothermal effects on multilayered composite plates using a refined higher order theory", *Compos. Struct.*, **92**(3), 633-646. https://doi.org/10.1016/j.compstruct.2009.09.034.

Madenci, E. and Özkılıç, Y.O. (2021), "Cyclic response of self-centering SRC walls with frame beams as boundary", *Steel Compos. Struct.*, **40**(2), 157-173. https://doi.org/10.12989/scs.2021.40.2.157.

Mantari, J.L. and Soares, C.G. (2013), "A novel higher-order shear deformation theory with stretching effect for functionally graded plates", *Compos. Part B: Eng.*, **45**(1), 268-281. https://doi.org/10.1016/j.compositesb.2012.05.036.

Mindlin, R. (1951), "Influence of rotatory inertia and shear on flexural motions of isotropic, elastic plates", https://doi.org/10.1115/1.4010217.

Mohammadimehr, M. and Meskini, M. (2020), "Analysis of porous micro sandwich plate: Free and forced vibration under magneto-electro-elastic loadings", *Adv. Nano Res.*, **8**(1), 69-82. http://dx.doi.org/10.12989/anr.2020.8.1.069.

Mudhaffar, I.M., Tounsi, A., Chikh, A., Al-Osta, M.A., Al-Zahrani, M.M. and Al-Dulaijan, S.U. (2021), « Hygro-thermo-mechanical bending behavior of advanced functionally graded ceramic metal plate resting on a viscoelastic foundation", *Structures*, **33**, 2177-2189. https://doi.org/10.1016/j.istruc.2021.05.090.

Nguyen, K., Thai, H.T. and Vo, T. (2015), "A refined higher-order shear deformation theory for bending, vibration and buckling analysis of functionally graded sandwich plates", *Steel Compos. Struct.*, **18**(1), 91-120. http://dx.doi.org/10.12989/scs.2015.18.1.091.

Pasternak, P.L. (1954), On a new method of analysis of an elastic foundation by means of two foundation constants", *Gos. Izd. Lit. po Strait i Arkh.*

Patel, B.P., Ganapathi, M. and Makhecha, D.P. (2002), "Hygrothermal effects on the structural behavior of thick composite laminates using higher-order theory", *Compos. Struct.*, **56**(1), 25-34. https://doi.org/10.1016/S0263-8223(01)00182-9.

Pham, Q.H., Nguyen, P.C. and Tran, V.K. (2024), "Effects of hygro-thermal environment on dynamic responses of variable thickness functionally graded porous microplates", *Steel Compos. Struct.*, **50**(5), 563-581. https://doi.org/10.12989/scs.2024.50.5.563.

Priyanka, R., Twinkle, C.M. and Pitchaimani, J. (2021), "Stability and dynamic behavior of porous FGM beam: influence of graded porosity, graphene platelets, and axially varying loads", *Eng. Comput.*, **38**, 4347-4366. https://doi.org/10.1007/s00366-021-01478-5.

Rabhi, M., Benrahou, K.H., Kaci, A., Houari, M.S.A., Bourada, F., Bousahla, A.A., Tounsi, A. and Adda Bedia, E.A. (2020), " A new innovative 3-unknowns HSDT for buckling and free vibration of exponentially graded sandwich plates resting on elastic foundations under various boundary conditions", *Geomech. Eng.*, **22**(2), 119-132. https://doi.org/10.12989/gae.2020.22.2.119.

Rahimi, A., Alibeigloo, A. and Safarpour, M. (2020), "Three-dimensional static and free vibration analysis of graphene platelet–reinforced porous composite cylindrical shell", *J. Vib. Control*, **26**(19-20), 1627-1645. https://doi.org/10.1177/1077546320902340.

Ram, K.S. and Sinha, P.K. (1991), "Hygrothermal effects on the bending characteristics of laminated composite plates", *Comput. Struct.*, **40**(4), 1009-1015. https://doi.org/10.1016/0045-7949(91)90332-G.

Rao, V.V.S. and Sinha, P.K. (2004), "Bending characteristic of thick multidirectional composite plates under hygrothermal environment", *J. Reinf. Plast. Comp.*, **23**(14), 1481-1495. https://doi.org/10.1177/0731684404038595.

Rostami, R. and Mohammadimehr, M. (2020), "Vibration control of rotating sandwich cylindrical shell-reinforced nanocomposite face sheet and porous core integrated with functionally graded magneto-electro-elastic layers", *Eng. Comput.*, 1-14. https://doi.org/10.1007/s00366-020-01052-5.

Sayyad, A.S. and Ghugal, Y.M. (2019), "Effects of nonlinear hygrothermomechanical loading on bending of FGM rectangular plates resting on two-parameter elastic foundation using four-unknown plate theory", *J. Therm. Stresses*, **42**(2), 213-232. https://doi.org/10.1080/01495739.2018.1469962.

Shankar, G., Kumar, S.K. and Mahato, P.K. (2017), "Vibration analysis and control of smart composite plates with delamination and under hygrothermal environment", *Thin-Wall. Struct.*, **116**, 53-68. https://doi.org/10.1016/j.tws.2017.03.013.

Sharma, H.K., Srivastava, M.C., Rajak, B., Singh, S., Verma, S., Kumar, R. and Singh, J. (2024), "Effect of porosity on stability analysis of bidirectional FGM skew plate via higher order shear deformation theory and RBF approach", *Int. J. Steel Struct.*, 1-13. https://doi.org/10.1007/s13296-024-00910-y.

Shen, H.S. (2001), "Hygrothermal effects on the postbuckling of shear deformable laminated plates", *Int. J. Mech. Sci.*, **43**(5), 1259-1281.

Thai, H.T. and Vo, T.P. (2013), "A new sinusoidal shear deformation theory for bending, buckling, and vibration of functionally graded plates", *Appl. Math. Model.*, **37**(5), 3269-3281. https://doi.org/10.1016/j.apm.2012.08.008.

Tlidji, Y., Benferhat, R. and Tahar, H.D. (2021), "Study and analysis of the free vibration for FGM microbeam containing various distribution shape of porosity", *Struct. Eng. Mech.*, **77**(2), 217-229. https://doi.org/10.12989/sem.2021.77.2.217.

Tounsi, A., Tahir, S.I., Al-Osta, M.A., Do-Van, T., Bourada, F., Bousahla, A.A. and Tounsi, A. (2023), "An integral quasi-3D computational model for the hygro-thermal wave propagation of imperfect FGM sandwich plates", *Comput. Concrete*, **32**(1), 61-74. https://doi.org/10.12989/cac.2023.32.1.061.

Tu, T.M., Quoc, T.H. and Long, N.V. (2017), "Bending analysis of functionally graded plates using new eight-unknown higher order shear deformation theory", *Struct. Eng. Mech.*, **62**(3), 311-324. https://doi.org/10.12989/sem.2017.62.3.311.

Turan, F. (2024) , "Free vibration response of multi-layered plates with trigonometrically distributed porosity based on the higher-order shear deformation theory", *Steel Compos. Struct.*, **53**(1), 77-90. https://doi.org/10.12989/scs.2024.53.1.077.

Wang, X., Dong, K. and Wang, X.Y. (2005), "Hygrothermal effect on dynamic interlaminar stresses in laminated plates with piezoelectric actuators", *Compos. Struct.*, **71**(2), 220-228. https://doi.org/10.1016/j.compstruct.2004.10.004.

Wattanasakulpong, N. and Ungbhakorn, V. (2014), "Linear and nonlinear vibration analysis of elastically restrained ends FGM beams with porosities", *Aerosp. Sci. Technol.*, **32**(1), 111-120. https://doi.org/10.1016/j.ast.2013.12.002.

Winkler, E. (1867), "Die Lehre von der Elastizitat and Festigkeit", Prag. *Dominicus*, 1867.

Yuksel, Y.Z. and Akbas, S.D. (2021), "Hygrothermal stress analysis of laminated composite porous plates", *Struct. Eng. Mech.*, **80**(1), 1-13. https://doi.org/10.12989/sem.2021.80.1.001.

Zenkour, A. (2013), "Hygrothermal analysis of exponentially graded rectangular plates", *J. Mech. Mater. Struct.*, **7**(7), 687-700. https://doi.org/10.2140/jomms.2012.7.687.

Zenkour, A.M. (2006). Generalized shear deformation theory for bending analysis of functionally graded plates", *Appl. Math. Model.*, **30**(1), 67-84.https://doi.org/10.1016/j.apm.2005.03.009.

Zghal, S., Frikha, A. and Dammak, F. (2017), "Static analysis of functionally graded carbon nanotube-reinforced plate and shell structures", *Compo. Struct.*, **176**, 1107-1123. https://doi.org/10.1016/j.compstruct.2017.06.015.

Zhang, Y., Guo, Z., Gong, Y., Shi, J., El Ouni, M.H. and Alhosny, F. (2023), "Elastic buckling performance of FG porous plates embedded between CNTRC piezoelectric patches based on a novel quasi 3D-HSDT in hygrothermal environment", *Adv. Nano Res.*, **15**(2), 175-189. https://doi.org/10.12989/anr.2023.15.2.175.

CC